Fitting-determined formulation of effective medium approximation for 3D trench structures in model-based infrared reflectrometry

Chuanwei Zhang,[1] Shiyuan Liu,[2,*] Tielin Shi,[1] and Zirong Tang[1]

[1]*Wuhan National Laboratory for Optoelectronics, Huazhong University of Science and Technology, Wuhan, Hubei, 430074, China*

[2]*State Key Laboratory of Digital Manufacturing Equipment and Technology, Huazhong University of Science and Technology, Wuhan, Hubei, 430074, China*

**Corresponding author: shyliu@mail.hust.edu.cn*

Received September 7, 2010; revised November 26, 2010; accepted December 14, 2010; posted December 16, 2010 (Doc. ID 134623); published February 1, 2011

The success of the model-based infrared reflectrometry (MBIR) technique relies heavily on accurate modeling and fast calculation of the infrared metrology process, which continues to be a challenge, especially for three-dimensional (3D) trench structures. In this paper, we present a simplified formulation for effective medium approximation (EMA), determined by a fitting-based method for the modeling of 3D trench structures. Intensive investigations have been performed with an emphasis on the generality of the fitting-determined (FD)-EMA formulation in terms of trench depth, trench pitch, and incidence angle so that its application is not limited to a particular configuration. Simulations conducted on a taper trench structure have further verified the proposed FD-EMA and demonstrated that the MBIR metrology with the FD-EMA-based model achieves an accuracy one order higher than that of the conventional zeroth-order EMA-based model. © 2011 Optical Society of America

OCIS codes: 120.0120, 300.6340, 050.6624, 050.2065.

1. INTRODUCTION

The demands on optical metrology of etched deep-trench structures continue to increase as microelectronic devices become more complex and three dimensional (3D). In recent years, the model-based infrared reflectrometry (MBIR) technique has been developed with unique advantages for the measurement of 3D deep-trench structures, and it has already been exploited in the application of dynamic random access memory (DRAM) and finfield-effect transistors (FinFETs) devices [1–3]. It is well recognized that the success of MBIR metrology relies heavily on accurate forward modeling and fast calculation of the infrared metrology process, which still remains a challenge, especially for 3D deep-trench structures. Rigorous coupled wave analysis (RCWA) [4–6] is ideally suited to simulate the optical response of periodic surface-relief structures and has been commonly used for modeling in scatterometry [7–9]. RCWA can achieve optical responses with very high accuracy, but its calculation is quite time consuming. Another attractive modeling method, effective medium approximation (EMA) [10–14], which provides more efficient computational ability than RCWA [15], has also been adopted to estimate the optical characteristics of deep-trench structures in MBIR [1]. EMA treats a periodic structure as a homogeneous medium and has been suggested for several applications, such as the design of diffractive optical elements (DOEs) [16–18] and the measurement of optical critical dimension (OCD) [19–21]. Although the optical response calculated with the EMA-based model may be slightly different from that with RCWA, it is much simpler for the forward modeling process of complex DOEs design and OCD measurement. As in the application of MBIR for metrology of periodic trench structures that correspond to advanced technology nodes in integrated circuit (IC) manufacturing, the trench structures are typically characterized by a pitch well into the submicrometer range and, thus, are much smaller than the optical wavelength in the mid-infrared that the MBIR technique performs [2]. The infrared light propagates through the trench structure as if it were a homogeneous medium with an effective permittivity that can be analytically determined from the geometry of the structure with an EMA approach.

Two main types of EMA have been adopted in MBIR: namely, zeroth-order EMA and second-order EMA. For two-dimensional (2D) trench structures, such as line/space test structures, that are widely used in the IC industry, zeroth-order EMA, taking a simple form in the static-limit regime, provides an acceptable modeling accuracy [2,11], while second-order EMA, with a closed form, achieves more accurate approximation [20,22]. Zeroth-order EMA of 2D trench structures in TE and TM polarization is expressed as

$$\varepsilon_{\parallel}^{0} = (1-f)\varepsilon_g + f\varepsilon_m, \tag{1}$$

$$\varepsilon_{\perp}^{0} = \frac{\varepsilon_g \varepsilon_m}{f\varepsilon_g + (1-f)\varepsilon_m}, \tag{2}$$

and second-order EMA is given by

$$\varepsilon_{\parallel}^{2} = \varepsilon_{\parallel}^{0} + \frac{\pi^2}{3} f^2 (1-f)^2 (\varepsilon_m - \varepsilon_g)^2 \left(\frac{\Lambda}{\lambda}\right)^2, \tag{3}$$

$$\varepsilon_{\perp}^{2} = \varepsilon_{\perp}^{0} + \frac{\pi^2}{3} f^2 (1-f)^2 \left(\frac{1}{\varepsilon_m} - \frac{1}{\varepsilon_g}\right)^2 (\varepsilon_{\perp}^{0})^3 \varepsilon_{\parallel}^{0} \left(\frac{\Lambda}{\lambda}\right)^2, \tag{4}$$

where $\varepsilon_{\parallel}^{0}$ and $\varepsilon_{\perp}^{0}$ are the zeroth-order effective permittivities of the trench structures for the electric field parallel and perpendicular to the trenches, respectively, $\varepsilon_{\parallel}^{2}$ and $\varepsilon_{\perp}^{2}$ are the second-order effective permittivities of the trench structures for the electric field parallel and perpendicular to the trenches, respectively, f is the void fraction of the trench structure, ε_g and ε_m are the permittivities of the trench material and the inclusion material, respectively, Λ is the trench pitch, and λ is the wavelength of the incidence beam.

For 3D trench structures, such as a square lattice of cylindrical trenches, the MBIR technique with an EMA-based modeling method has a special advantage because it is possible to perform in-chip metrology of the 3D trench structures rather than using the line/space test structures mentioned earlier. In comparison with EMA for 2D trench structures, the no-static EMA solution with a closed form has been developed for 3D trench structures. As in the metrology of 3D trench structures by MBIR, the expression of EMA given by Eq. (1) is adopted for TE polarization, and another zeroth-order EMA, a Maxwell–Gamett-type formulation, is adopted for TM polarization [2]:

$$\varepsilon_{\perp} = \varepsilon_1 \left[1 - f \frac{2(\varepsilon_g - \varepsilon_m)}{\varepsilon_g + \varepsilon_m + f(\varepsilon_g - \varepsilon_m)} \right]. \tag{5}$$

Unfortunately, the zeroth-order EMA formulations given by Eqs. (1) and (5) have been demonstrated to provide only a rough approximation for 3D trench structures [22].

There are several other analytical formulations of EMA that have been reported for modeling 3D periodic structures in applications other than deep-trench metrology with MBIR. Jackson and Coriell derived the upper and lower bounds of the zeroth-order effective permittivity for 3D periodic structures, and their method can achieve acceptable approximation only for structures with similar optical indices of the composed materials [23]. Motamedi *et al.* proposed an approximate solution by averaging the two zeroth-order effective permittivities of a 2D periodic structure in TE and TM polarization so that the 3D problem is converted into a 2D one [24], but their solution has been demonstrated to be quite inaccurate [25]. Lalanne and Lalanne presented a rigorous formulation of the second-order effective refractive index based on the Fourier decomposition of the wave propagating along the direction perpendicular to the 3D periodic structures [26]. Although this method provides a good approximation for the infrared spectroscopic ellipsometry [27], the rigorous solution to the zeroth- and second-order term coefficients of the second-order EMA formulation requires the inversion of infinite matrices, which limits its application in the nonlinear regression for fast parameter extraction in MBIR.

In 2006, Moon and Kim developed a fitting-based method for the determination of the effective permittivity of 1D metallic gratings [28] and successfully applied it to the optimal design of photonic crystals [29]. The effective permittivity was obtained by fitting to the reflectance characteristic calculated by the RCWA, and this fitting-based method could yield correct results that were not achievable through analytical EMA formulations. Therefore, the numerical fitting-based method may provide another choice for the determination of effective permittivity of subwavelength periodic structures. Motivated by its success in the modeling for optimal design of 1D metallic gratings, we attempt to explore its potential in the modeling of MBIR metrology of 3D deep-trench structures. Instead of directly fitting only one parameter (namely, the effective permittivity), as in the case of 1D gratings in [28], we propose a simplified formulation with two parameters (namely, zeroth- and second-order term coefficients) to calculate the effective refractive index for 3D deep-trench structures, and then we apply the fitting-based method to determine these two parameters. This fitting-determined (FD)-EMA formulation, particularly suitable for 3D trench structures, can be considered as an approximate expression of the rigorous solution of the second-order EMA derived in [26]. This is the main point of our improvement. In our previous work [22], a similar FD-EMA formulation was simply introduced and successfully applied to a bottle trench structure in MBIR metrology. In this paper, we present the FD-EMA formulation with sufficient details and perform further intensive investigations with an emphasis on the possibility of generalizing the FD-EMA formulation in terms of trench depth, trench pitch, and incidence angle so that its application is not limited to a particular configuration. As an example, we conduct simulations on a 3D taper trench structure to further verify the usefulness of the FD-EMA formulation for MBIR metrology.

The remainder of this paper is organized as follows. Section 2 introduces the FD-EMA formulation and describes in detail how to determine it for 3D deep-trench structures. Section 3 investigates the applicability of the FD-EMA formulation in 3D deep-trench modeling for MBIR metrology. Section 4 presents a simulated study to apply the FD-EMA formulation to the 3D taper trench metrology and demonstrates its high accuracy. Finally, we draw some conclusions in Section 5.

2. FD-EMA FORMULATION

In the fabrication of microelectronic devices, such as DRAM and FinFETs, high-aspect ratio cavities are etched on a silicon substrate to form the charge-storage capacitors, and the MBIR technique has been introduced for process control of this fabrication step. Therefore, a simple 3D trench structure is considered to derive the FD-EMA formulation as depicted in Fig. 1(a), where a vertical trench array is formed on a silicon substrate with a depth of H, equal trench pitches of Λ in the x and y directions, and equal trench widths of W in the x and y directions. Since the cross section of the 3D trench structure in microelectronic devices is usually designed to be circular or square, we narrow the following discussion to centrally symmetric trench structures. The refractive indices of the incidence medium (air) and the substrate material (silicon) are set to be n_i and n_s, respectively. In the setup of MBIR, the wave probes on the trench structure with an incidence angle θ of 45° and an azimuthal angle φ of 0°, and the wavelength λ of interest ranges in the mid-infrared from 2 to 20 μm. For a large wavelength-to-pitch ratio, if an effective medium exists such that the trench structure of Fig. 1(a) is functionally equivalent to that of Fig. 1(b), in which a single, homogeneous film of an equal thickness is layered on the silicon substrate, the effective permittivity ε_{eff} of the effective medium can be expanded in a power series [11]:

$$\varepsilon_{\text{eff}} = \varepsilon_0 + \varepsilon_1 \alpha^{-1} + \varepsilon_2 \alpha^{-2} + \ldots, \tag{6}$$

where $\alpha = \lambda/\Lambda$ is the wavelength-to-pitch ratio, ε_0 is the square of the zeroth-order effective refractive index, and ε_i, $i = 1, \ldots, N$ represents the ith-order term coefficient of the series expansion. As derived in [26], the odd-order terms in the power series can be omitted, and only the zeroth- and

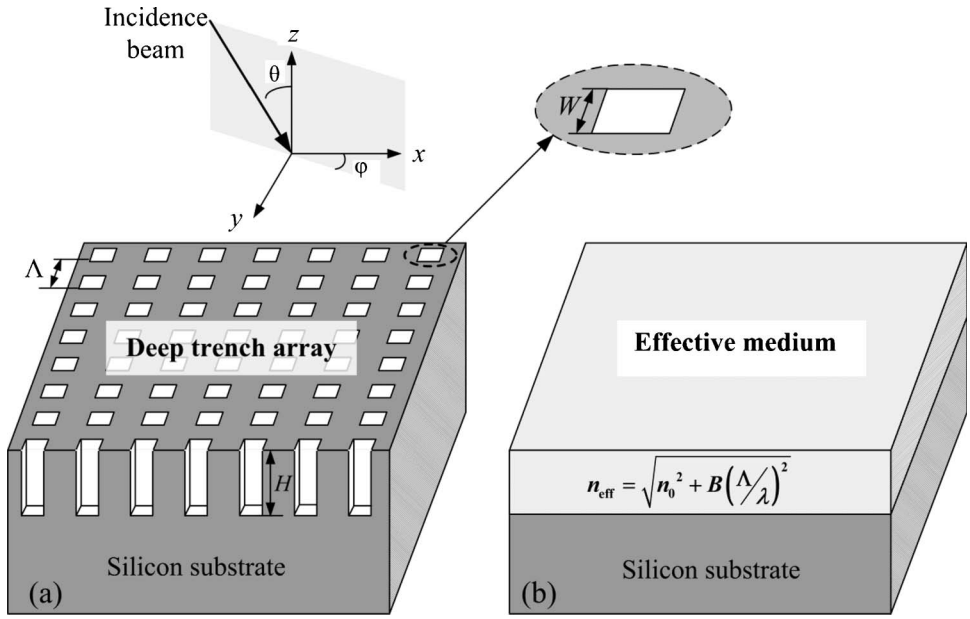

Fig. 1. (a) 3D trench structure and (b) its effective optical model. The incidence beam probes on the trench structure with the incidence angle θ and azimuthal angle φ.

second-order terms are retained for second-order EMA. This rigorous expression of the zeroth- and second-order term coefficients is obtained by using the Fourier series expansion method. However, the rigorous derivation requires solving the inversion of infinite matrices; thus, the computation of solving the inverse problem is extremely time consuming. Here, we employ the fitting-based method to obtain the approximate expression of the zeroth- and second-order term coefficients of the series expansion. We substitute the refractive index for the permittivity and simplify the power series into the following FD-EMA formulation:

$$n_{\text{eff}} = \sqrt{n_0^2 + B\left(\frac{\Lambda}{\lambda}\right)^2}, \tag{7}$$

where n_{eff} and n_0 represent the second- and zeroth-order effective refractive indices, respectively, and the second-order term coefficient ε_2 is substituted by B for simplicity.

In general, n_0 and B mainly depend on the relative permittivity and the void faction of the trench structures. For a certain trench structure to be measured by MBIR, the permittivities of the composed materials are *a priori* knowledge and can be determined in advance, hence, n_0 and B are affected only by the void fraction f. We employ the fitting-based method to determine the approximate expressions of n_0 and B as a function of f. At the very beginning, an equal-thickness effective medium model of the 3D deep-trench structure is established, and the effective refractive index of the effective medium is described by the FD-EMA formulation, as shown in Fig. 1(b). The procedure to determine the approximate expressions of n_0 and B is shown in Fig. 2 and described in detail as follows.

Step 1: the reflectance R_r of the 3D trench structure in Fig. 1(a) is simulated with the 2D RCWA [6]. With a compromise to achieve a balance between accuracy and time consumption, we employ about 10×10 spatial harmonics, which obtain an average relative error of less than 0.05% as compared with the simulated results using 50×50 spatial harmonics in the mid-infrared wavelength range.

Step 2: the reflectance R_s of the effective medium model in Fig. 1(b) is calculated using the Fresnel coefficients equation [30]:

$$R_s = \left|\frac{r_1 e^{j\delta} + r_2 e^{-j\delta}}{e^{j\delta} + r_1 r_2 e^{-j\delta}}\right|^2, \tag{8}$$

where

$$r_1 = \frac{n_{\text{i}} \cos\theta_1 - n_{\text{eff}} \cos\theta_2}{n_{\text{i}} \cos\theta_1 + n_{\text{eff}} \cos\theta_2}, \qquad r_2 = \frac{n_{\text{eff}} \cos\theta_2 - n_s \cos\theta_3}{n_{\text{eff}} \cos\theta_2 + n_s \cos\theta_3}, \tag{9}$$

$$\delta = 2\pi H n_{\text{eff}} \cos\theta_2 / \lambda. \tag{10}$$

Here, θ_1, θ_2, and θ_3 denote the incidence angle in the incidence medium, the effective medium, and the substrate,

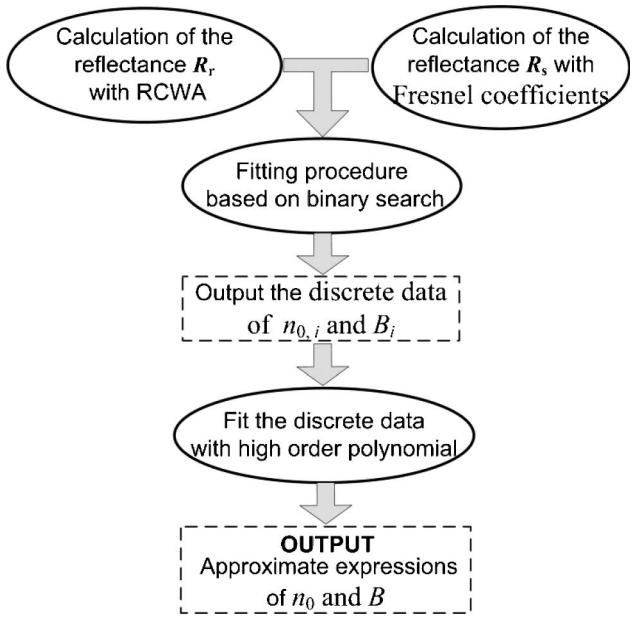

Fig. 2. Flow chart for determining the approximate expressions of n_0 and B.

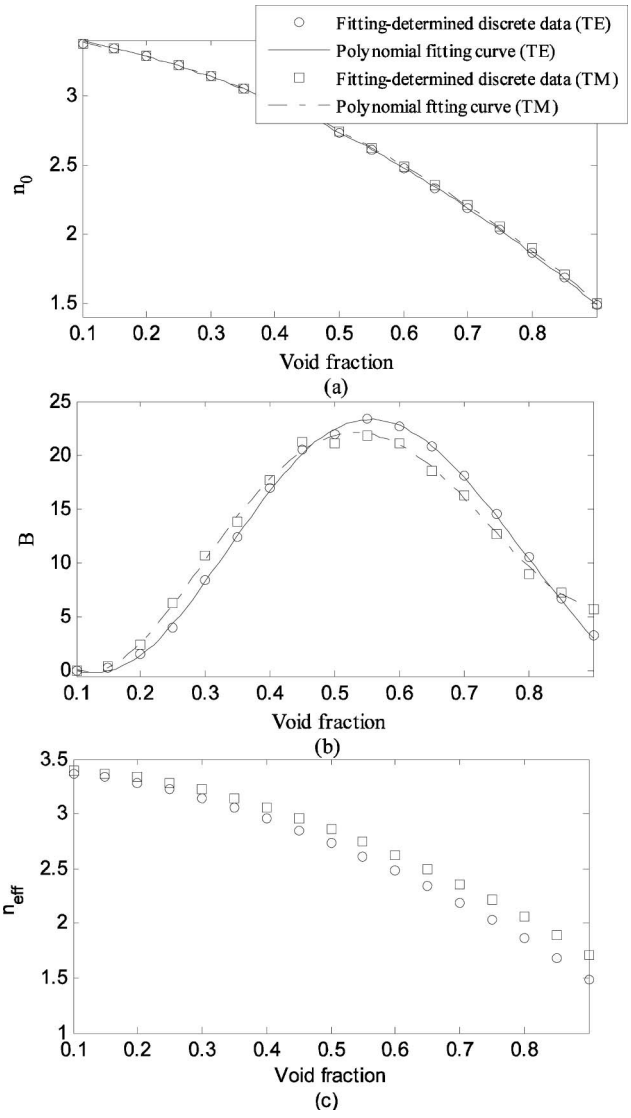

Fig. 3. FD discrete data (circles and squares) and the best-fitted polynomial curves (solid and dashed curves) of (a) zeroth-order effective refractive, (b) second-order term coefficient, and (c) second-order effective refractive in the FD-EMA formulation for TE and TM polarization.

respectively, and they are related by Snell's law. The above calculating process of R_s is used for the fitting procedure in Step 3.

Step 3: the zeroth-order effective refractive index $n_{0,i}$ and the second-order term coefficient B_i at the void fraction f_i are obtained by a fitting procedure based on a binary search, through all possible combinations of $n_{0,i}$ and B_i in a given range, where i represents the sequence number of the void fraction that is taken into account. This results in an optimal pair that minimizes the deviation between R_r and R_s.

Table 1. Polynomial Coefficients of the Best-Fitting Curve of the Zeroth-Order Effective Refractive Index in TE and TM Polarization

	a_0	a_1	a_2
TE	3.462	−0.545	−1.831
TM	3.450	−0.489	−1.848

Table 2. Polynomial Coefficients of the Best-Fitting Curve of the Second-Order Term Coefficient in TE and TM Polarization

	b_0	b_1	b_2	b_3	b_4	b_5	b_6
TE	3.127	−25.81	280.7	3034	−7193	6593	−2136
TM	9.354	−177.6	980.7	−1359	159.6	624.4	−226.8

Step 4: the void fraction f_i varies in the range considered, and then the corresponding $n_{0,i}$ and B_i are obtained with the above fitting procedure.

Step 5: a high-order polynomial is adopted as an attempt to fit the discrete data of $n_{0,i}$ and B_i, and the approximate expressions of n_0 and B as the functions of f are achieved by the following expressions:

$$n_0 = a_0 + a_1 f + a_2 f^2 + \ldots + a_j f^j$$
$$B = b_0 + b_1 f + b_2 f^2 + \ldots + b_k f^k, \tag{11}$$

where a_j and b_k are the polynomial coefficients to be determined by the least squares method, and j and k represent the highest polynomial orders.

3. APPLICABILITY OF FD-EMA IN 3D TRENCH MODELING

A. Modeling of a 3D Trench Structure

Figure 3 shows the FD discrete data of n_0, B, and n_{eff} and their best-fitting polynomial curves in both TE and TM polarization for 3D trench structures with $n_i = 1$, $n_s = 3.4$, $H = 4\,\mu$m, $\Lambda = 0.2\,\mu$m, and W varying from 0.02 to 0.18 μm (i.e., f varying from 10% to 90%). The discrete data of n_0 and B are obtained by the fitting-based method described in Section 2, and then best fitted by a second-order polynomial and a sixth-order polynomial, respectively. We achieve the final solutions of a_i and b_i, as shown in Tables 1 and 2, with the least squares method. From Figs. 3(a) and 3(b), we find that the best-fitted polynomial curves of n_0 in TE and TM polarization are almost in coincidence with each other, and the best-fitted polynomial curves of B are slightly different from each other for TE and TM polarization. It is also noted in Fig. 3(c) that the n_{eff} calculated with the FD discrete data of n_0 and B shows acceptable continuity, which indicates that n_0 and B are the global solutions in the fitting-based method.

To estimate the modeling accuracy with FD-EMA, simulations have been carried out in different polarization states at the void fractions of 20%, 40%, 60%, and 80%. The simulation results are obtained with four models, including RCWA, FD-EMA by Eq. (7), zeroth-order EMA by Eqs. (1) and (5), and second-order EMA by Eqs. (3) and (4). As shown in Fig. 4, it can be noted that the FD-EMA-based model achieves a satisfactory accuracy of approximation as compared with the rigorous calculations in both TE and TM polarizations. The modeling accuracy with the proposed FD-EMA formulation has been dramatically improved as compared with both zeroth-order EMA and second-order EMA.

B. Independence Investigation

The approximate expressions of the zeroth-order effective refractive index n_0 and the second-order term coefficient B in the FD-EMA formulation are determined at certain trench depth, trench pitch, and incidence angle. Therefore, it is

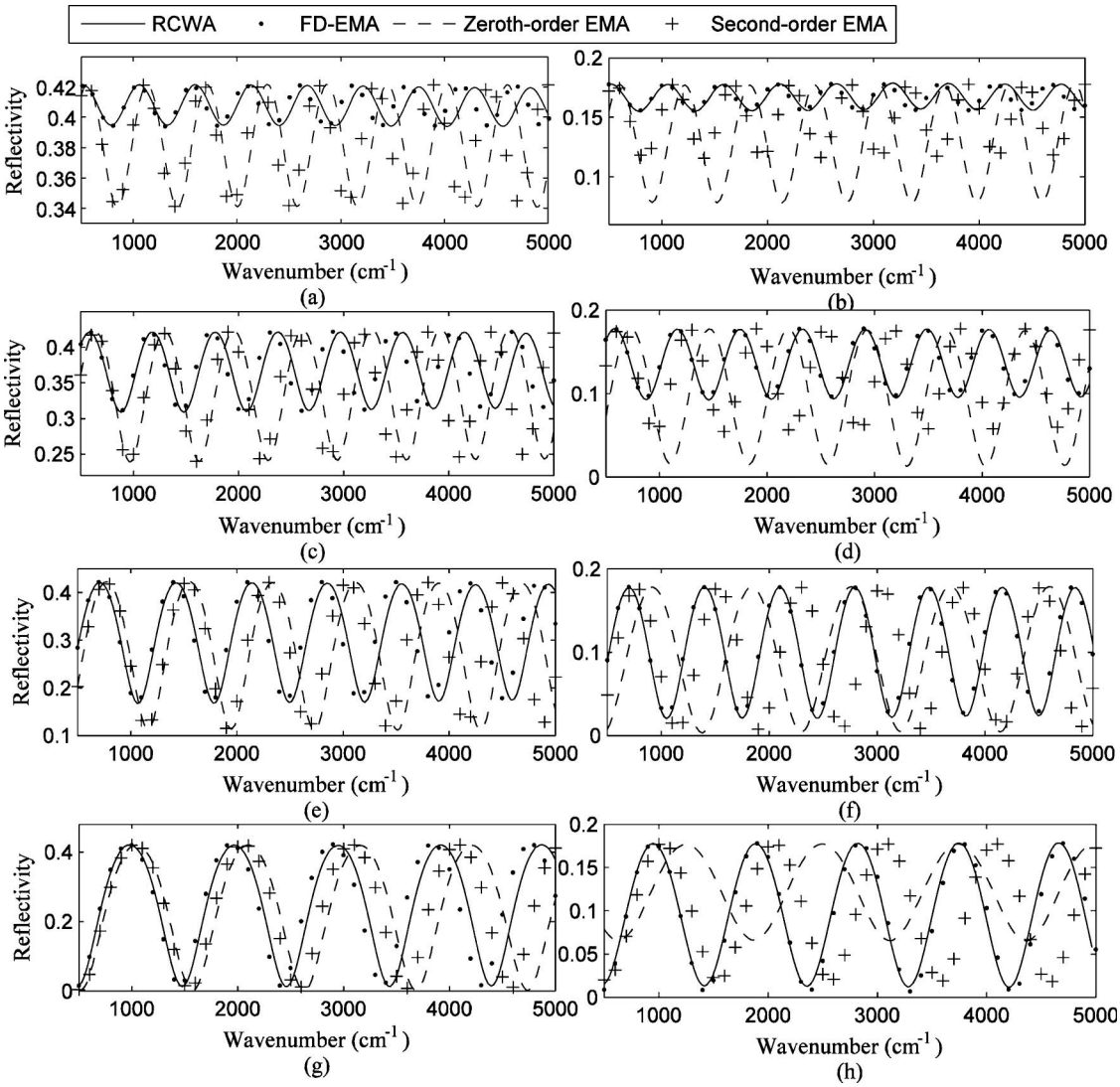

Fig. 4. Reflectance spectra calculated by RCWA, the FD-EMA-based model, the zeroth-order EMA-based model, and second-order EMA at the void fractions of (a) 20% in TE polarization, (b) 20% in TM polarization, (c) 40% in TE polarization, (d) 40% in TM polarization, (e) 60% in TE polarization, (f) 60% in TM polarization, (g) 80% in TE polarization, and (h) 80% in TM polarization. The trench parameters for the simulation: trench depth is 4 μm and trench pitch is 0.2 μm.

necessary to investigate the independence of n_0 and B on the three parameters mentioned above. We have determined n_0 and B with one of the three parameters varying while the other parameters are fixed. Figures 5–7 show the simulated results performed on the 3D trench structure in Fig. 1. For simplicity, all the simulations have been performed for TE polarization.

First, a numerical analysis has been performed to investigate the independence of the FD-EMA formulation on the trench depth. The trench depth varies from 0.01 to 10 μm. The trench pitch is fixed at 0.2 μm, the incidence angle is fixed at 45°, and the void fraction is set at 20%, 40%, 60%, and 80%, respectively, for each simulation. The discrete data of n_0 and B at each trench depth are determined by the fitting-based method described in Section 2, and the simulation results are shown in Fig. 5. It is clear that n_0 remains almost constant as the trench depth varies, and B also remains constant at the trench depth range, especially for high void fraction.

A similar study has been performed to investigate the independence of the FD-EMA formulation on the trench pitch. The trench pitch varies from 0.04 to 0.2 μm with an increment of 0.04 μm, the trench depth is fixed at 5 μm, the incidence angle is fixed at 45°, and the void fraction is set at 20%, 40%, 60%, and 80%, respectively, for each simulation. Figure 6 shows the FD discrete data of n_0 and B in each fixed void fraction, respectively. It is noted that n_0 almost remains unchanged as the trench pitch varies, while B changes as the trench pitch varies.

Finally, the independence of the FD-EMA formulation on the incidence angle has been investigated with the geometry of the 3D trench structure fixed and the incidence angle varied from 0° to 80° with an increment of 10°. For each simulation, the trench depth is fixed at 5 μm, the trench pitch is fixed at 0.2 μm, and the void fraction is set at 20%, 40%, 60%, and 80%, respectively. From the simulation results in Fig. 7, it is observed that both n_0 and B remain almost constant as the incidence angle varies.

These investigations evaluated the impact of the three considered parameters on n_0 and B, and the simulated results reveal that n_0 is almost independent of the three parameters while B is partly affected by them. It is noted from Eq. (7) that n_0 is the main factor to influence the accuracy of the

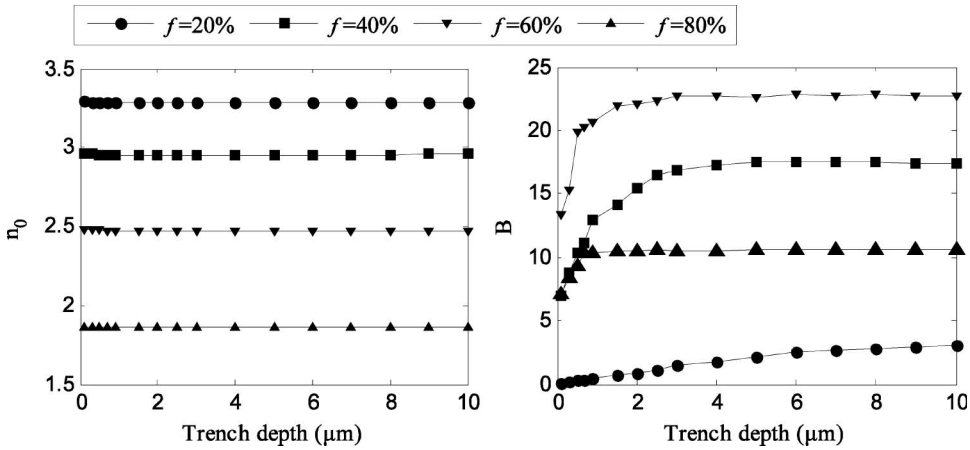

Fig. 5. Zeroth-order refractive index n_0 and the second-order term coefficient B in different trench depths calculated by the fitting-based method. The void fraction f is set at 20%, 40%, 60%, and 80%, respectively.

calculated effective refractive index, and B can be considered as a corrected factor that only plays a role in the short wavelength range. From this point of view, the FD-EMA formulation is independent of the considered parameters and guarantees its generality; thus, its application will not be limited to a particular configuration.

C. Accuracy Evaluation

In metrology by MBIR, the accuracy of parameter extraction depends on the forward modeling accuracy. As in the forward modeling process, the EMA-based model provides an approximate value of the reflectance spectrum that can be rigorously calculated by RCWA. To further evaluate the modeling error of the FD-EMA-based model, we performed a quantitative analysis with the average absolute relative error (AARE) given by

$$\mathrm{AARE} = \frac{\sum_{i=1}^{N} |[R_r(\lambda_i) - R_s(\lambda_i)]/R_r(\lambda_i)|}{N} \times 100\%, \qquad (12)$$

where N is the total number of wavelength points λ_i at which the calculation is performed. The AARE evaluates the overall discrepancy of the reflectance spectrum calculated by the FD-EMA-based model and RCWA. Figures 8–10 show the simulation results of AARE versus the trench depth, the trench pitch, and the incidence angle, respectively, and the simulations are performed with the same conditions shown as in Figs. 5–7, respectively.

As shown in Fig. 8, the maximal AARE for the trench depth appears at the minimal depth for each simulation. This observation agrees with the simulation result in Fig. 5, in which a significant variation arises for B in the small trench depth range. However, the maximum of AARE at the trench depth of 0.1 μm is less than about 0.5%, which indicates that FD-EMA is not only applicable to deep-trench structures, but also to shallow trench structures. This capability is particularly useful for the modeling of taper trench structures, which need to be divided into multiple thin layers. The application of FD-EMA to a taper trench structure is further discussed in Section 4.

Figure 9 represents the AARE for variable trench pitches. As the trench pitch decreases from 0.2 to 0.04 μm, the AARE increases and reaches a maximum of less than 2%. The result reveals that the FD-EMA formulation determined at a certain trench pitch is also applicable for variable trench pitch. However, it is necessary to carry out a different FD-EMA formulation for different technique nodes to achieve more accurate modeling results.

Figure 10 depicts the AARE as a function of the incidence angle. As the incidence angle varies from 0° to 80°, the AARE varies below 0.35%, which indicates that the

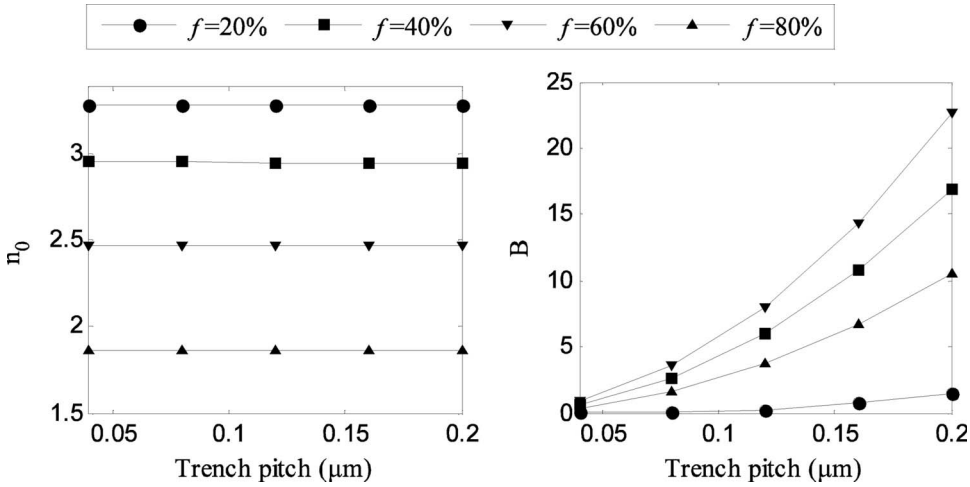

Fig. 6. Zeroth-order effective refractive index n_0 and the second-order term coefficient B in different trench pitches calculated by the fitting-based method. The void fraction f is set at 20%, 40%, 60%, and 80%, respectively.

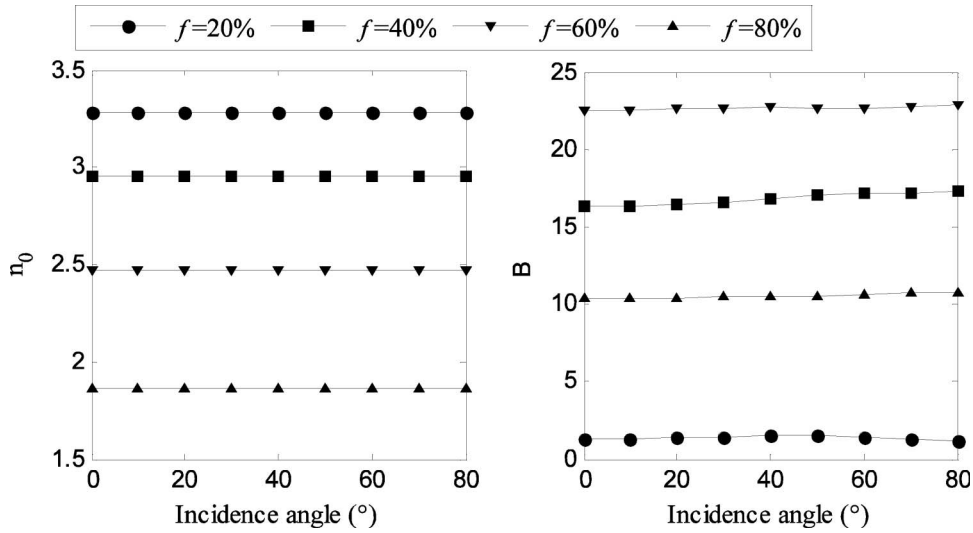

Fig. 7. Zeroth-order refractive index n_0 and the second-order term coefficient B with variable incidence angle calculated by the fitting-based method. The void fraction f is set at 20%, 40%, 60%, and 80%, respectively.

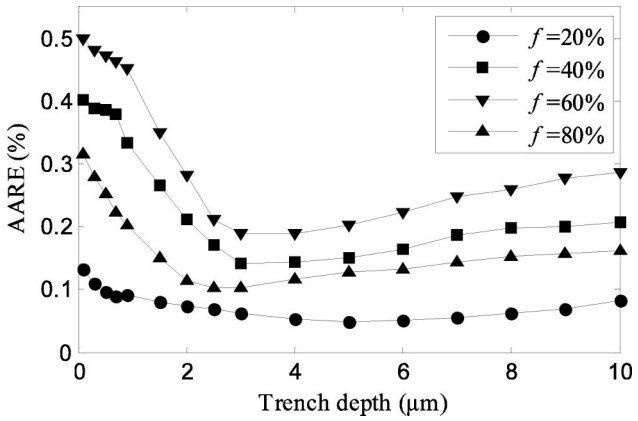

Fig. 8. AARE of the FD-EMA-based model as a function of the trench depth at the void fractions of 20%, 40%, 60%, and 80%.

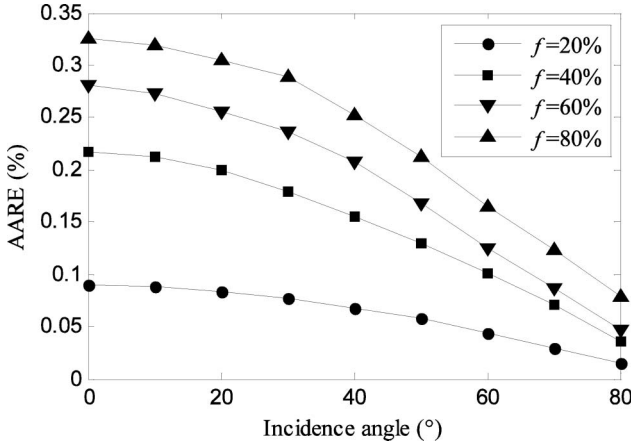

Fig. 10. AARE of the FD-EMA-based model as a function of the incidence angle at the void fractions of 20%, 40%, 60%, and 80%.

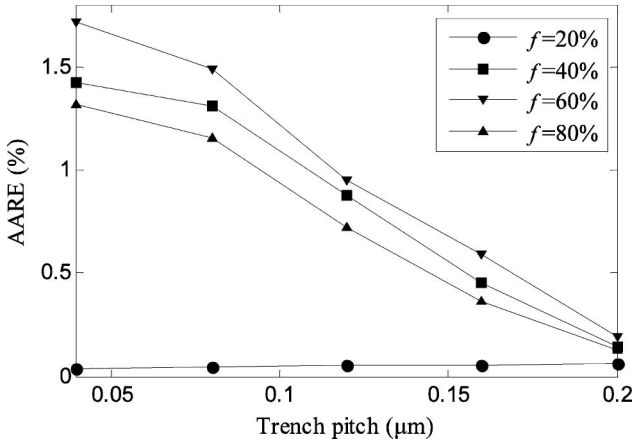

Fig. 9. AARE of the FD-EMA-based model as a function of the trench pitch at the void fractions of 20%, 40%, 60%, and 80%.

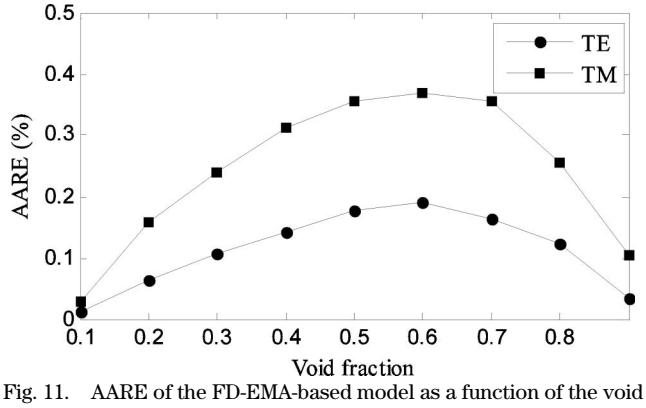

Fig. 11. AARE of the FD-EMA-based model as a function of the void fraction for TE and TM polarization.

FD-EMA formulation determined at a certain incidence angle is applicable to different incidence angles. This observation will be useful for the MBIR setup with variable incidence angle, although, in MBIR, the incidence angle is usually chosen around the Brewster's angle.

Finally, we estimate the modeling accuracy with the FD-EMA formulation in different polarization. The AARE as a function of void fraction is carried out as shown in Fig. 11. It is noted that the FD-EMA-based model achieves more accurate results in the TE polarization than in the TM polarization. When the void fraction varies from 10% to 90%, the FD-EMA-based model produced an AARE lower than 0.4%.

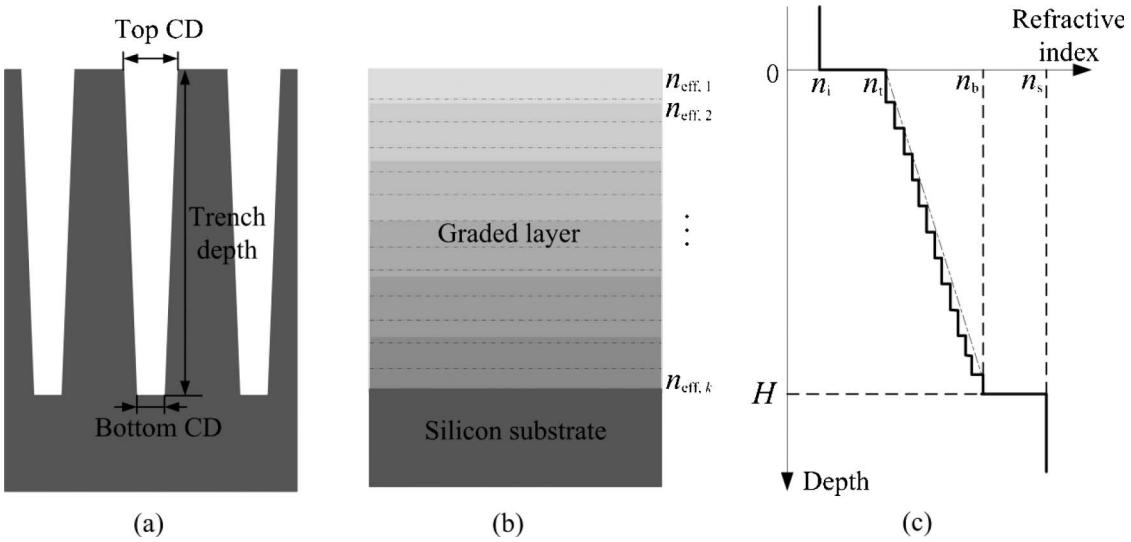

Fig. 12. (a) Structure of the 3D taper trenches etched on the silicon substrate, (b) its effective medium model, and (c) its effective refractive index versus the depth.

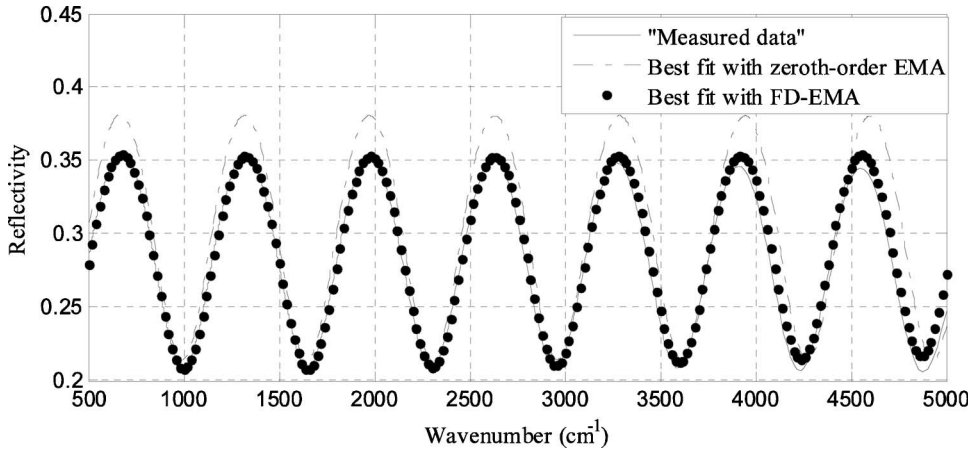

Fig. 13. Measured data of the taper trench simulated by RCWA and the best-fit spectra with zeroth-order EMA and the FD-EMA-based model. The trench parameters for the simulation: trench depth is 3 μm, top CD is 0.1 μm, bottom CD is 0.075 μm, and trench pitch is 0.18 μm.

Table 3. Comparison of the Extraction Error of Zeroth-Order EMA and the FD-EMA-Based Model

	Trench Depth		Top CD		Bottom CD	
Trench Parameters	Error (nm)	Relative Error (%)	Error (nm)	Relative Error (%)	Error (nm)	Relative Error (%)
Zeroth-order EMA	3.1	0.1	4.1	4.1	3.5	4.6
FD-EMA	1.6	0.05	0.26	0.26	0.19	0.25

4. APPLICATION OF FD-EMA IN 3D TRENCH METROLOGY

In order to evaluate its applicability for actual 3D deep-trench structures, we further apply FD-EMA to fast parameter extraction for MBIR metrology through a simulation test. The RCWA simulated spectrum is considered to be the "measured data," and then the geometric parameters of the trench structure are extracted from the measured data with the artificial neural network and Levenberg–Marquardt combined method proposed in our previous work [22]. As a comparison, the forward modeling in solving the inverse problem of parameter extraction is performed based on FD-EMA and the zeroth-order EMA in Eqs. (1) and (5), respectively. In our previous work, a similar FD-EMA formulation was simply introduced and applied to a bottle trench structure with a satisfactory result [22]. In this paper, the simulated test is performed on a 3D taper trench structure to further validate the proposed FD-EMA formulation.

As shown in Fig. 12(a), the 3D taper trench structure consists of a tapered layer with gradually varying width as the depth increases. The trench depth is designed to be 3 μm, the trench pitch is designed to be 0.18 μm, and the top critical dimension (CD) and the bottom CD are designed to be 100 and 75 nm, respectively. With the EMA method, the taper trench layer is modeled as a graded effective layer with the refractive index varying linearly from n_t to n_b, as shown in Figs. 12(b) and 12(c). Here, n_t and n_b represent the refractive index on

the top and bottom interfaces, respectively. The graded layer is divided into k thin layers with the refractive index linearly varying from $n_{\text{eff},1}$ to $n_{\text{eff},k}$, while $n_{\text{eff},1}$ and $n_{\text{eff},k}$ are equal to n_t and n_b, respectively. The effective refractive index of each divided layer is calculated with the FD-EMA formulation and zeroth-order EMA formulation, respectively. Then, the forward reflectivity calculation of the effective medium model in Figure 10b is carried out with the propagation matrix method of multiple-layered media [31].

Figure 13 depicts the "measured spectrum" simulated by RCWA, together with the best-fit spectrum calculated with zeroth-order EMA and the best-fit spectrum calculated by FD-EMA. The extracted parameters are shown in Table 3. When compared with zeroth-order EMA, the FD-EMA-based model has achieved more accurate results, especially for the trench width (i.e., the top CD and bottom CD). The simulated test shows that the accuracy of the extracted result produced by the FD-EMA-based model is one order higher than that of zeroth-order EMA.

5. CONCLUSIONS

In this paper, we present an FD-EMA formulation for modeling 3D deep-trench structures in MBIR metrology. The applicability of the FD-EMA formulation to arbitrary trench depth, trench pitch, and incidence angle has been intensively investigated, and the results reveal the generality of FD-EMA for variable optical configurations and structural changes. A further quantitative analysis has been performed to evaluate the modeling error of the FD-EMA-based model for variable configurations and has achieved satisfactory results. The FD-EMA formulation has been applied to the parameter extraction process of the MBIR metrology for a taper trench structure, and the simulation work demonstrates that FD-EMA achieves an accuracy one order higher than zeroth-order EMA. FD-EMA is expected to be useful in the fast and accurate modeling of 3D deep-trench structures for MBIR metrology as well as in other applications.

ACKNOWLEDGMENTS

The authors wish to acknowledge financial support from the National Natural Science Foundation of China (NSFC; grants 91023032, 51005091, 50775090), the Fundamental Research Funds for the Central Universities of China (grant 2010ZD004), and the Postdoctoral Science Foundation of China (grant 20100470052).

REFERENCES

1. P. A. Rosenthal, C. A. Durán, J. Tower, and A. Mazurenko, "Model-based infrared metrology for advanced technology nodes and 300 mm wafer processing," AIP Conf. Proc. **788**, 620–624 (2005).
2. A. A. Maznev, A. Mazurenko, C. A. Durán, and M. Gostein, "Measuring trench structures for microelectronics with model-based infrared reflectometry," AIP Conf. Proc. **931**, 74–78 (2007).
3. C. A. Durán, A. A. Maznev, G. T. Merklin, A. Mazurenko, and M. Gostein, "Infrared reflectometry for metrology of trenches in power devices," in *Proceedings of IEEE Conference on Advanced Semiconductor Manufacturing* (IEEE, 2007), pp. 175–179.
4. R. Petit, *Electromagnetic Theory of Gratings* (Springer-Verlag, 1980).
5. L. Li, "New formulation of the Fourier modal method for crossed surface-relief gratings," J. Opt. Soc. Am. A **14**, 2758–2767 (1997).
6. P. Lalanne, "Improved formulation of the coupled-wave method for two-dimensional gratings," J. Opt. Soc. Am. A **14**, 1592–1598 (1997).
7. C. J. Raymond, M. R. Murnane, S. L. Prins, S. S. H. Naqvi, J. W. Hosch, and J. R. McNeil, "Multiparameter grating metrology using optical scatterometry," J. Vac. Sci. Technol. B **15**, 361–368 (1997).
8. X. Niu, N. Jakatdar, J. Bao, and C. J. Spanos, "Specular spectroscopic scatterometry," IEEE Trans. Semicond. Manuf. **14**, 97–111 (2001).
9. P. Reinig, R. Dost, M. Mort, T. Hingst, U. Mantz, J. Moffitt, S. Shakya, C. J. Raymond, and M. Littau, "Metrology of deep trench etched memory structures using 3D scatterometry," Proc. SPIE **5752**, 559–569 (2005).
10. T. C. Choi, *Effective Medium Theory: Principles and Applications* (Oxford University, 1999).
11. S. M. Rytov, "Electromagnetic properties of a finely stratified medium," Sov. Phys. JETP **2**, 466–475 (1956).
12. H. Kikuta, H. Yoshida, and K. Iwata, "Ability and limitation of effective medium theory for subwavelength gratings," Opt. Rev. **2**, 92–99 (1995).
13. H. Kikuta, Y. Ohira, H. Kubo, and K. Iwata, "Effective medium theory of two-dimensional subwavelength gratings in the nonquasi-static limit," J. Opt. Soc. Am. A **15**, 1577–1585 (1998).
14. P. Lalanne and J. P. Hugonin, "High-order effective-medium theory of subwavelength gratings in classical mounting: application to volume holograms," J. Opt. Soc. Am. A **15**, 1843–1851 (1998).
15. D. H. Raguin and G. M. Morris, "Antireflection structured surfaces for the infrared spectral region," Appl. Opt. **32**, 1154–1167 (1993).
16. H. Kikuta, Y. Ohira, and K. Iwata, "Achromatic quarter-wave plates using the dispersion of form birefringence," Appl. Opt. **36**, 1566–1572 (1997).
17. W. Yu, K. Takahara, T. Konishi, T. Yotsuya, and Y. Ichioka, "Fabrication of multilevel phase computer-generated hologram elements based on effective medium theory," Appl. Opt. **39**, 3531–3536 (2000).
18. W. Freese, T. Kämpfe, E. B. Kley, and A. Tünnermann, "Design of binary subwavelength multiphase level computer generated holograms," Opt. Lett. **35**, 676–678 (2010).
19. A. Weidner, M. Slodowski, C. Halm, C. Schneider, and L. Pfitzner, "Effective-medium model for fast evaluation of scatterometric measurements on gratings," Proc. SPIE **5375**, 232–243 (2004).
20. I. Abdulhalim, "Simplified optical scatterometry for periodic nanoarrays in the near-quasi-static limit," Appl. Opt. **46**, 2219–2228 (2007).
21. B. C. Bergner, T. A. Germer, and T. J. Suleski, "Effective medium approximations for modeling optical reflectance from gratings with rough edges," J. Opt. Soc. Am. A **27**, 1083–1090 (2010).
22. C. W. Zhang, S. Y. Liu, T. L. Shi, and Z. R. Tang, "Improved model-based infrared reflectometry for measuring deep trench structures," J. Opt. Soc. Am. A **26**, 2327–2335 (2009).
23. J. L. Jackson and S. R. Coriell, "Transport coefficients of composite materials," J. Appl. Phys. **39**, 2349–2354 (1968).
24. M. E. Motamedi, W. H. Southwell, and W. J. Gunning, "Antireflection surfaces in silicon using binary optics technology," Appl. Opt. **31**, 4371–4376 (1992).
25. E. B. Grann, M. G. Moharam, and D. A. Pommet, "Artificial uniaxial and biaxial dielectrics with use of two-dimensional subwavelength binary gratings," J. Opt. Soc. Am. A **11**, 2695–2703 (1994).
26. P. Lalanne and D. L. Lalanne, "On the effective medium theory of subwavelength periodic structure," J. Mod. Opt. **43**, 2063–2085 (1996).
27. P. Y. Guittet, U. Mantz, and P. Weidner, "Infrared spectroscopic ellipsometry in semiconductor manufacturing," Proc. SPIE **5375**, 771–778 (2004).
28. S. Moon and D. Kim, "Fitting-based determination of an effective medium of a metallic periodic structure and application to photonic crystals," J. Opt. Soc. Am. A **23**, 199–207 (2006).
29. S. Moon and D. Kim, "Investigation of an effective medium theory for metallic periodic structure," Proc. SPIE **6128**, 61281M (2006).
30. M. Born and E. Wolf, *Principles of Optics* (Cambridge University, 1999).
31. P. Yeh, *Optical Waves in Layered Media* (Wiley, 1988).